ISSN 1674-1056
http://cpb.iphy.ac.cn
http://iopscience.iop.org/cpb
中国物理 B Chinese Physics
中国物理 Chinese Physics B

A macroscopic traffic model based on weather conditions

Zawar H. Khan, Syed Abid Ali Shah, T. Aaron Gulliver

Citation: Chin. Phys. B . 2018, 27(7): 070202. **doi:** 10.1088/1674-1056/27/7/070202

Journal homepage: http://cpb.iphy.ac.cn; http://iopscience.iop.org/cpb

What follows is a list of articles you may be interested in

An extension of integrable equations related to AKNS and WKI spectral problems and their reductions

Xian-Guo Geng(耿献国), Yun-Yun Zhai(翟云云)

Chin. Phys. B . 2018, 27(4): 040201. **doi:** 10.1088/1674-1056/27/4/040201

Integrability classification and exact solutions to generalized variable-coefficient nonlinear evolution equation

Han-Ze Liu(刘汉泽), Li-Xiang Zhang(张丽香)

Chin. Phys. B . 2018, 27(4): 040202. **doi:** 10.1088/1674-1056/27/4/040202

Constructing (2+1)-dimensional *N*=1 supersymmetric integrable systems from the Hirota formalism in the superspace

Jian-Yong Wang(王建勇), Xiao-Yan Tang(唐晓艳), Zu-Feng Liang(梁祖峰)

Chin. Phys. B . 2018, 27(4): 040203. **doi:** 10.1088/1674-1056/27/4/040203

Improved reproducing kernel particle method for piezoelectric materials

Ji-Chao Ma(马吉超), Gao-Feng Wei(魏高峰), Dan-Dan Liu(刘丹丹)

Chin. Phys. B . 2018, 27(1): 010201. **doi:** 10.1088/1674-1056/27/1/010201

Improved control for distributed parameter systems with time-dependent spatial domains utilizing mobile sensor—actuator networks

Jian-Zhong Zhang(张建中), Bao-Tong Cui(崔宝同), Bo Zhuang(庄波)

Chin. Phys. B . 2017, 26(9): 090201. **doi:** 10.1088/1674-1056/26/9/090201

A macroscopic traffic model based on weather conditions*

Zawar H. Khan[1,†], Syed Abid Ali Shah[2], and T. Aaron Gulliver[2]

[1] Department of Electrical Engineering, University of Engineering and Technology, Peshawar, Pakistan
[2] Department of Electrical and Computer Engineering, University of Victoria, PO Box 1700, STN CSC, Victoria, BC Canada

(Received 20 November 2017; revised manuscript received 4 April 2018; published online 25 June 2018)

A traffic model based on the road surface conditions during adverse weather is presented. The surface of a road is affected by snow, compacted snow, and ice, which affects the traffic behavior. In this paper, a new macroscopic traffic flow model based on the transition velocity distribution is proposed which characterizes traffic alignment under adverse weather conditions. Two examples are considered to illustrate the effect of the transition velocity behavior on traffic velocity and density. Simulation results are presented which show that this model provides a more accurate characterization of traffic flow behavior than the well known Payne–Whitham model. The proposed model can be used to reduce accidents and improve road safety during adverse weather conditions.

Keywords: macroscopic traffic flow, anticipation, Payne–Witham (PW) model, adverse weather

PACS: 02.30.Jr, 02.60.Cb **DOI:** 10.1088/1674-1056/27/7/070202

1. Introduction

Weather has a significant effect on traffic flow and impacts traffic mobility, planning, and efficiency. During normal weather conditions, the traffic alignment is smooth as vehicles cover distances quickly to align. In adverse weather conditions, traffic alignment is affected by the surface conditions of the road. Snow, ice, and/or compacted snow can make the pavement slick. This reduces the friction between the tires and road, so vehicles require longer distances and more time to align than in normal weather. The alignment in adverse weather has an effect on traffic flow. Vehicles move slowly due to reduced friction and thus are more likely to form clusters.[1,2] The reduced friction and smaller distances between vehicles in the clusters are the leading cause of accidents in adverse weather conditions.[3]

A realistic characterization of traffic is required to reduce accidents and mitigate congestion on roads.[4] Adverse weather conditions such as rain, fog, dust, snow, and ice reduce visibility, friction, and vehicle maneuverability which cause delays and speed variability. An 18% increase in delay has been observed on roads in adverse weather.[5] In snow, when the temperature is above 0 °C, the injury rate is increased by 6.6% compared to in normal weather, and by 15% when the temperature is below 0 °C. In heavy rain when the temperature is moderate, i.e., between 0 °C and 20 °C, the traffic volume increases by 12%, but increases by only 8.5% when the temperature is less than 0 °C and by 6.5% when the temperature is greater than 20 °C.

Road safety is a major concern of every country. Accidents cause serious injuries and loss of life as well as property damage. According to the World Health Organization, 1.24 million road fatalities occurred during 2013 worldwide,[6] and accident rates are highest when the temperature is below freezing and in snowy weather. A single collision can cause multiple or chain reaction accidents, and this is more prevalent in adverse weather conditions. Light snow can cause slippery pavement with vehicle traction reduced by roughly 10%.[7] On the other hand, heavy snowfall and rainfall reduce visibility and thus increase the time and distance to align, reducing speeds by 16% to 40%. The speed declines by 30% to 40% during a snowfall and with snowy or slushy pavement.[8] Accident rates have been shown to increase from 100% to 1000% during snowfall.[9] There was a 20% increase in road accidents during the winter season in Ottawa, Canada, from 1990 to 1998.[6] Snow affects driving behavior more compared to other adverse weather conditions. The reason is that snow affects both visibility and road traction. If the temperature is low on the day after a heavy snowfall or high precipitation, there is low traction due to reduced friction. Furthermore, snow covers lane markings and road signs which are designed to aid drivers, which leads to a higher accident rate.[10] There is an increase in fuel consumption and travel delay in snow and ice conditions.[11] Traffic speeds were reduced by 3% to 5% with light snow and 30% to 40% with heavy snow on a freeway in Canada.[12] A study of a busy freeway in Minnesota stated that in snow there is a speed reduction of 40%, a decrease in maximum traffic flow of 11%, and an increase in traffic alignment time from 2 s to 3 s.[13]

There are three main types of traffic flow models: macroscopic, microscopic, and mesoscopic. Microscopic models represent single vehicle position and velocity, while macroscopic models represent system-level characteristics. A meso-

*Project supported by Higher Education Commission, Pakistan/National Center of Big Data and Cloud Computing.
†Corresponding author. E-mail: zawarkhan@nwfpuet.edu.pk
© 2018 Chinese Physical Society and IOP Publishing Ltd

scopic model shares the properties of both microscopic and macroscopic models. Vehicles are modeled at an individual level while the traffic flow behavior is averaged. A macroscopic traffic flow model considers speed and density to determine the cumulative behavior of traffic. The density ρ is the average number of vehicles on a road segment per unit length. The product of speed (velocity) v and density ρ determines the traffic flow per unit time. Lighthill, Whitham, and Richards[14,15] developed a macroscopic traffic flow model (known as the LWR model), which is based on the equilibrium flow of vehicles. This model assumes that vehicles align in zero time and ignores the transition velocity during alignment.[16] Payne and Witham[17] independently developed a two-equation model for traffic flow, which is known as the Payne–Whitham (PW) model. The first equation is the continuity equation for the conservation of vehicles on a road, while the second models the acceleration behavior of traffic based on driver presumption, relaxation, and traffic acceleration. Driver presumption is based mainly on changes in the forward traffic density, while relaxation characterizes the alignment of traffic during transitions. The PW model is known to produce oscillatory behavior at traffic discontinuities. This is stop-and-go traffic due to changes in traffic density during transitions and is typical in congestion. The traffic flow is assumed to be adjusted with a constant speed (velocity), which can produce unrealistic results such as velocities below zero, which are impossible. Due to the instability of the PW model, it is unable to accurately predict traffic clusters and their densities.[18]

Traffic flow behavior has been characterized based on the road surface conditions. For example, the spatiotemporal flow behavior on a flat road is different than that on a hilly road.[19–24] The speed (velocity) varies as the slope changes and this can cause accidents and congestion.[25,26] Further, the slope angle and length have a significant effect on traffic flow,[27] e.g., traffic oscillations increase with the downhill slope and and are inversely proportional to the uphill slope.[19]

This paper presents a characterization of traffic flow during adverse weather conditions based on road surface conditions such as snow, compacted snow, and ice. Traffic flow transitions occur due to a change in speed, and are affected by weather conditions. The transition velocity is derived for traffic during the alignment of flow at transitions. The distribution of this velocity is obtained based on the road surface conditions which are characterized by a severity index. This index is high for low friction caused by snow, compacted snow, and ice and the velocity during transitions should be low for safe alignment. The effect of this transition velocity is incorporated in the proposed macroscopic traffic flow model. This model is evaluated on a circular road to demonstrate the alignment of vehicles in adverse weather conditions. Results are presented which show that this model accurately characterizes the traffic flow during alignment. The flow has smaller variations than with the PW model, which indicates reduced acceleration and deceleration in adverse weather.

The rest of this paper is organized as follows. In Section 2, the transition velocity distribution based on the weather conditions is derived. Then, a macroscopic traffic flow model is presented which employs this distribution. Section 3 describes the decomposition of both the proposed and PW models using the Roe scheme. The Jacobian matrix of both models is developed to obtain the corresponding eigenvalues, eigenvectors, and average velocities. The proposed and PW models are evaluated and compared in Section 4. The spatial and temporal evolution of traffic flow, velocity, and density are presented for a circular road under different weather conditions. Finally, some conclusions are given in Section 5.

2. Traffic flow models

Payne and Witham[17] independently developed a two-equation model for traffic flow which is known as the PW model. The first equation is

$$\frac{\partial \rho}{\partial t} + \frac{\partial (\rho v)}{\partial x} = 0. \tag{1}$$

This is a conservation relation which indicates that the traffic flow remains conserved and there are no transitions on the road. In this case, no alignment is required for the traffic flow. The assumptions are that the road length is infinite and there is no acceleration or deceleration. The second equation is

$$\frac{\partial (\rho v)}{\partial t} + \frac{v \partial v}{\partial x} = \frac{C_0^2}{\rho}\frac{\partial \rho}{\partial x} + \left(\frac{v(\rho) - v}{\tau}\right). \tag{2}$$

This indicates that there is acceleration and deceleration because of ingress and egress from the flow. When transitions occur, alignment takes place during the relaxation time τ. C_0 is the velocity constant and τ is the relaxation time to align velocities during transitions. $\frac{v(\rho)-v}{\tau}$ is called the relaxation term and $v(\rho)$ is the equilibrium velocity distribution which is dependent on the density. According to the relaxation term, the traffic adjusts to this distribution. Several models have been proposed for $v(\rho)$.[28] A commonly employed model is the Greenshields model,[29,30] which is given by

$$v(\rho) = v_{\mathrm{m}}\left(1 - \frac{\rho}{\rho_{\mathrm{m}}}\right). \tag{3}$$

The anticipation term is

$$\frac{C_0^2}{\rho}\frac{\partial \rho}{\partial x}, \tag{4}$$

which accounts for spatial changes in the traffic density. It is a function of the spatial gradient of density $\partial\rho/\partial x$. The anticipation term of the PW model cannot characterize the spatial change in density in different weather conditions due to the velocity constant. Thus, with the PW model drivers are alike and behave the same in all conditions.

Adverse weather conditions such as snow, compacted snow, and ice have a significant impact on the traffic flow. There is reduction in the speed (velocity) due to reduced friction between the tires and road surface. The effect of weather can be characterized by a severity index which is given by[31]

$$\beta = \frac{d_s}{f_s} + D_c \frac{d_c}{f_c} + D_i \frac{d_i}{f_i}, \tag{5}$$

where d_s, d_i, and d_c are the depth of snow, ice, and compacted snow on the road, respectively. f_s, f_c, and f_i are the corresponding tire friction coefficients, and D_c and D_i are the density ratios of compacted snow and ice to new snow, respectively. The distance covered by a vehicle to align its velocity during a transition is known as the distance headway. The time to cover this distance is known as the time headway. The minimum distance required for safe alignment between vehicles under normal weather conditions is the safe distance headway H, and the time to cover this distance is the safe time headway α. In adverse weather, velocity is reduced due to lower friction on the road and can be characterized as

$$v_t(\beta) = \frac{H}{\alpha}\left(1 - \frac{\beta}{\beta_m}\right), \tag{6}$$

where β_m is the maximum severity index. When $\beta = \beta_m$, the transition velocity is zero as there is minimum friction between the tires and road. When there is no snow, compacted snow, or ice on the road and the surface of the road is clear, $\beta = 0$ and the weather is considered normal. In normal weather, the transition velocity only depends on the safe distance and safe time headways, i.e., $v_t = H/\alpha$. The transition velocity parameters are summarized in Table 1.

Table 1. Transition velocity parameters.

Weather	Severity index β	Transition velocity v_t
Worst	β_m	0
Normal	0	H/α

During adverse weather, the changes in traffic are based on the road conditions. A driver will align with a smaller velocity in adverse weather than in normal weather to avoid an accident. The transition velocity $v_t(\beta)$ is aligned during the relaxation time τ so the rate at which the density changes is $v_t(\beta)/\tau$. For a faster traffic flow, τ is smaller and the alignment is quicker. The relaxation time is the traffic alignment sensitivity, and traffic alignment is less sensitive for a larger relaxation time.

For the PW model, driver anticipation is characterized by the velocity constant C_0, so behavior is fixed for all transition conditions including adverse weather. This model does not account for traffic behavior based on the surface condition of the road. Thus, to better characterize this behavior a variable anticipation term based on the road condition is introduced. To achieve this, C_0^2 in Eq. (4) is replaced with $\frac{\partial}{\partial x}\left(\frac{v_t(\beta)}{\tau}\right)$ to obtain

$$\frac{1}{\rho}\frac{\partial}{\partial x}\left(\frac{v_t(\beta)}{\tau}\right)\frac{\partial \rho}{\partial x}. \tag{7}$$

Substituting Eq. (6) in Eq. (7) gives the anticipation term

$$\frac{\partial}{\rho \partial x}\left(\frac{\frac{H}{\alpha}\left(1 - \frac{\beta}{\beta_m}\right)}{\tau}\right)\frac{\partial \rho}{\partial x}. \tag{8}$$

This accounts for the spatial changes in density due to the weather conditions. For a smaller τ, a larger change in the density occurs during transitions, so traffic alignment is faster and achieves a smooth flow in less time. The flow due to egress and ingress with the PW model is characterized by the relaxation term $[v(\rho) - v]/\tau$ in Eq. (2). According to this term, the traffic flow aligns based on the equilibrium velocity distribution, which is based on the traffic density distribution. The equilibrium velocity is large for a small density and vice versa. In the proposed model, the traffic aligns based on the transition velocity distribution $[\frac{H}{\alpha}\left(1 - \frac{\beta}{\beta_m}\right)]/\tau$ which considers the surface conditions and safe headway. The transition velocity is maximum for normal surface conditions, i.e., $\beta = 0$, and the traffic aligns based on $(H/\alpha)/\tau$. In the PW model, large abrupt changes in the traffic flow occur due to the unrealistic constant C_0 in the anticipation term, which results in traffic oscillations. The relaxation term is used to smooth these changes. However, in the proposed model, the changes in flow are based on realistic road conditions and the relaxation is not required to smooth the changes.

Substituting Eq. (7) in Eq. (2) gives the acceleration relation based on the transition velocity distribution for the proposed model which is

$$\frac{\partial(\rho v)}{\partial t} + \frac{v \partial v}{\partial x} = \frac{\partial}{\rho \partial x}\left(\frac{\frac{H}{\alpha}\left(1 - \frac{\beta}{\beta_m}\right)}{\tau}\right)\frac{\partial \rho}{\partial x}, \tag{9}$$

and in normal weather conditions this is

$$\frac{\partial(\rho v)}{\partial t} + \frac{v \partial v}{\partial x} = \frac{\partial}{\rho \partial x}\left(\frac{\frac{H}{\alpha}}{\tau}\right)\frac{\partial \rho}{\partial x}. \tag{10}$$

The first equation of the proposed model is the same as that in the PW model.

3. Roe decomposition technique

High resolution discretization of the traffic flow model is required to achieve accurate solutions. The high-order schemes employed for LWR traffic flow models are able to capture large discontinuities and achieve accurate solutions. The complexity of these schemes can be reduced using relaxation,[32] so that the Jacobian matrix and eigenvalues are not required.[33] The relaxation based on weighted essentially non oscillatory (WENO) finite difference schemes was used to obtain accurate solutions for inhomogeneous traffic

flows.[34] However, WENO techniques cannot capture large abrupt discontinuities.[35] Roe decomposition approximates the large discontinuities and has been shown to provide consistent and accurate results for vehicular and pedestrian traffic flow models.[36] Therefore in this paper, the proposed and PW models are discretized using Roe decomposition[37] to evaluate their performance.

The Roe technique is used to approximate a nonlinear system of equations

$$\boldsymbol{G}_t + \boldsymbol{f}(\boldsymbol{G})_x = \boldsymbol{S}(\boldsymbol{G}), \tag{11}$$

where $\boldsymbol{G}$ is the vector of data variables, $\boldsymbol{f}(\boldsymbol{G})$ is the vector of functions of the data variables, and $\boldsymbol{S}(\boldsymbol{G})$ is the vector of source terms. The subscripts t and x denote the partial derivatives with respect to time and distance, respectively. Equation (11) can be expressed as

$$\frac{\partial \boldsymbol{G}}{\partial t} + \frac{\partial \boldsymbol{f}}{\partial \boldsymbol{G}}\frac{\partial \boldsymbol{G}}{\partial x} = \boldsymbol{S}(\boldsymbol{G}), \tag{12}$$

where $\partial \boldsymbol{f}/\partial \boldsymbol{G}$ is the gradient of the function of data variables with respect to these variables. Let $\boldsymbol{A}(\boldsymbol{G})$ be the Jacobian matrix of the system so that Eq. (12) can be written as

$$\frac{\partial \boldsymbol{G}}{\partial t} + \boldsymbol{A}(\boldsymbol{G})\frac{\partial \boldsymbol{G}}{\partial x} = \boldsymbol{S}(\boldsymbol{G}). \tag{13}$$

Setting the source term to zero gives the quasilinear form

$$\frac{\partial \boldsymbol{G}}{\partial t} + \boldsymbol{A}(\boldsymbol{G})\frac{\partial \boldsymbol{G}}{\partial x} = 0. \tag{14}$$

The Roe technique is used to linearize the Jacobian matrix $\boldsymbol{A}(\boldsymbol{G})$ by decomposing it into eigenvalues and eigenvectors. It is based on the concept that the data variables, eigenvalues, and eigenvectors remain conserved for small changes in time and distance. This technique is widely employed because it is able to capture the effects of abrupt changes in the data variables. The data variables in the PW and proposed models are density ρ and flow ρv.

Consider a road divided into M equidistant segments and N equal duration time steps. The total length is x_M so a segment has length $\delta x = x_M/M$, and the total time duration is t_N, so a time step is $\delta t = t_N/N$. The Jacobian matrix is approximated for road segments $(x_i + \frac{\delta x}{2}, x_i - \frac{\delta x}{2})$. This matrix is obtained for all M segments in every time interval (t_{n+1}, t_n), where $t_{n+1} - t_n = \delta t$. Let $\Delta \boldsymbol{G}$ denote the change in the data variables $\boldsymbol{G}$, and $\Delta \boldsymbol{f}$ the corresponding change in the functions of these variables. Furthermore, let $\boldsymbol{G}_i$ be the average values of the data variables in the ith segment. The change in flux at the boundary between the ith and $(i+1)$th segments is defined as

$$\Delta \boldsymbol{f}_{i+\frac{1}{2}} = \boldsymbol{A}(\boldsymbol{G}_{i+\frac{1}{2}})\Delta \boldsymbol{G}, \tag{15}$$

where $\boldsymbol{A}(\boldsymbol{G}_{i+\frac{1}{2}})$ is the Jacobian matrix at the segment boundary and $\boldsymbol{G}_{i+\frac{1}{2}}$ is the vector of data variables at the boundary obtained using the Roe technique. The flux approximates the change in traffic density and flow at the segment boundary so that

$$\Delta \boldsymbol{f}_{i+\frac{1}{2}} = \boldsymbol{A}(\boldsymbol{G}_{i+\frac{1}{2}})(\boldsymbol{G}_{i+1} - \boldsymbol{G}_i), \tag{16}$$

where the approximation $\Delta \boldsymbol{G} = (\boldsymbol{G}_{i+1} - \boldsymbol{G}_i)$ is used. The flux at the boundary between segments i and $i+1$ at time n can then be approximated by

$$\boldsymbol{f}^n_{i+\frac{1}{2}}(\boldsymbol{G}^n_i, \boldsymbol{G}^n_{i+1}) = \frac{1}{2}\left(\boldsymbol{f}(\boldsymbol{G}^n_i) + \boldsymbol{f}(\boldsymbol{G}^n_{i+1})\right) - \frac{1}{2}\Delta \boldsymbol{f}_{i+\frac{1}{2}}, \tag{17}$$

where $\boldsymbol{f}(\boldsymbol{G}^n_i)$ and $\boldsymbol{f}(\boldsymbol{G}^n_{i+1})$ denote the values of the functions of the data variables in road segments i and $i+1$, respectively, at time n. Substituting Eq. (16) into Eq. (17) gives

$$\begin{aligned}\boldsymbol{f}^n_{i+\frac{1}{2}}(\boldsymbol{G}^n_i, \boldsymbol{G}^n_{i+1}) = {} & \frac{1}{2}\left(\boldsymbol{f}(\boldsymbol{G}^n_i) + \boldsymbol{f}(\boldsymbol{G}^n_{i+1})\right) \\ & - \frac{1}{2}\boldsymbol{A}(\boldsymbol{G}_{i+\frac{1}{2}})\left(\boldsymbol{G}^n_{i+1} - \boldsymbol{G}^n_i\right).\end{aligned} \tag{18}$$

This approximates the change in density and flow without considering the source. The updated data variables are obtained by including the source term, which gives

$$\boldsymbol{G}^{n+1}_i = \boldsymbol{G}^n_i - \frac{\delta t}{\delta x}\left(\boldsymbol{f}^n_{i+\frac{1}{2}} - \boldsymbol{f}^n_{i-\frac{1}{2}}\right) + \delta t \boldsymbol{S}(\boldsymbol{G}^n_i). \tag{19}$$

4. Jacobian matrix

In this section, the Jacobian matrix $\boldsymbol{A}(\boldsymbol{G})$ is derived. We first consider the PW model and convert it into conservation form giving

$$v\rho_t + v(\rho v)_x = 0, \tag{20}$$

where the subscripts t and x denote the partial derivatives with respect to time and distance, respectively. Then

$$(\rho v)_t = \rho v_t + v\rho_t, \tag{21}$$

and rearranging gives

$$v\rho_t = (\rho v)_t - \rho v_t. \tag{22}$$

Substituting Eq. (22) into Eq. (20), we obtain

$$\rho v_t = v(\rho v)_x + (\rho v)_t. \tag{23}$$

Multiplying Eq. (2) by ρ gives

$$\rho v_t + \rho v v_x + C_0^2 \rho_x = \rho \frac{v(\rho) - v}{\tau}, \tag{24}$$

and substituting Eq. (23) in Eq. (24) results in

$$v(\rho v)_x + (\rho v)_t + \rho v v_x + C_0^2 \rho_x = \rho \frac{v(\rho) - v}{\tau}. \tag{25}$$

We have

$$(\rho v v)_x = v(\rho v)_x + \rho v v_x, \tag{26}$$

and rearranging gives

$$v(\rho v)_x = (\rho vv)_x - \rho vv_x. \tag{27}$$

Substituting Eq. (27) in Eq. (25), we obtain

$$(\rho vv)_x + (\rho v)_t + C_0^2\rho_x = \rho\frac{v(\rho)-v}{\tau}. \tag{28}$$

Now, using the fact that

$$(\rho vv)_x = \left(\frac{(\rho v)^2}{\rho}\right)_x,$$

Eq. (28) can be written as

$$(\rho v)_t + \left(\frac{(\rho v)^2}{\rho} + C_0^2\rho\right)_x = \rho\left(\frac{v(\rho)-v}{\tau}\right), \tag{29}$$

which is in conservation form. The source term can be considered as traffic movement into (ingress) and out of (egress) the traffic flow. If the source term is assumed to be zero and the traffic mobility is conserved, then the right hand side of Eq. (29) is zero, so

$$(\rho v)_t + \left(\frac{(\rho v)^2}{\rho} + C_0^2\rho\right)_x = 0. \tag{30}$$

The model in quasilinear form is then

$$\boldsymbol{G} = \begin{pmatrix}\rho\\ \rho v\end{pmatrix}, \quad \boldsymbol{f}(\boldsymbol{G}) = \begin{pmatrix}f_1\\ f_2\end{pmatrix} = \begin{pmatrix}\rho v\\ \frac{(\rho v)^2}{\rho} + C_0^2\rho\end{pmatrix},$$
$$\boldsymbol{S}(\boldsymbol{G}) = \begin{pmatrix}0\\ 0\end{pmatrix}. \tag{31}$$

The Jacobian matrix $\boldsymbol{A}(\boldsymbol{G}) = \partial f/\partial G$ from Eq. (31) is

$$\boldsymbol{A}(\boldsymbol{G}) = \begin{pmatrix}0 & 1\\ -\frac{(\rho v)^2}{\rho^2} + C_0^2 & \frac{2\rho v}{\rho}\end{pmatrix}, \tag{32}$$

which gives

$$\boldsymbol{A}(\boldsymbol{G}) = \begin{pmatrix}0 & 1\\ -v^2 + C_0^2 & 2v\end{pmatrix}. \tag{33}$$

The eigenvalues λ_i of the Jacobian matrix are required to obtain the flux in Eq. (18), and are obtained from Eq. (33) as the solution of

$$\left|\boldsymbol{A}(\boldsymbol{G}) - \lambda\boldsymbol{I}\right| = \begin{vmatrix}-\lambda & 1\\ -v^2 + C_0^2 & 2v-\lambda\end{vmatrix} = 0, \tag{34}$$

which gives

$$\lambda^2 - 2v\lambda + v^2 - C_0^2 = 0. \tag{35}$$

The eigenvalues are then

$$\lambda_{1,2} = \frac{2v \pm \sqrt{4v^2 - 4(v^2 - C_0^2)}}{2} = v \pm \sqrt{C_0^2}. \tag{36}$$

For the PW model

$$\lambda_{1,2} = v \pm C_0. \tag{37}$$

For the proposed model, we have

$$C_0^2 = \int \frac{\partial}{\partial x}\left(\left(\frac{H(1-\frac{\beta}{\beta_m})}{\alpha\tau}\right)\right) \mathrm{d}x$$

and substituting this in Eq. (30) gives the eigenvalues

$$\lambda_{1,2} = v \pm \sqrt{\left(\frac{H(1-\frac{\beta}{\beta_m})}{\alpha\tau}\right)}. \tag{38}$$

The eigenvectors are obtained by solving

$$|\boldsymbol{A}(\boldsymbol{G}) - \lambda\boldsymbol{I}|x = 0, \tag{39}$$

where

$$\boldsymbol{x} = \begin{pmatrix}1\\ x_2\end{pmatrix}. \tag{40}$$

For the PW model, using Eq. (33) and $\lambda_1 = v + C_0$ from Eq. (37), the eigenvectors are obtained from Eq. (39) as

$$\boldsymbol{e}_1 = \begin{pmatrix}1\\ v + C_0\end{pmatrix}, \tag{41}$$

$$\boldsymbol{e}_2 = \begin{pmatrix}1\\ v - C_0\end{pmatrix}. \tag{42}$$

For the proposed model, using Eq. (33) and $\lambda_1 = v + \sqrt{\left(\frac{H(1-\frac{\beta}{\beta_m})}{\alpha\tau}\right)}$ from Eq. (38), equation (39) takes the form

$$\begin{pmatrix}-v - \sqrt{\left(\frac{H(1-\frac{\beta}{\beta_m})}{\alpha\tau}\right)} & 1\\ \left(\frac{H(1-\frac{\beta}{\beta_m})}{\alpha\tau}\right) - v^2 & v - \sqrt{\left(\frac{H(1-\frac{\beta}{\beta_m})}{\alpha\tau}\right)}\end{pmatrix}\begin{pmatrix}1\\ x_2\end{pmatrix} = 0, \tag{43}$$

so the eigenvectors are

$$\boldsymbol{e}_1 = \begin{pmatrix}1\\ v + \sqrt{\left(\frac{H(1-\frac{\beta}{\beta_m})}{\alpha\tau}\right)}\end{pmatrix}, \tag{44}$$

$$\boldsymbol{e}_2 = \begin{pmatrix}1\\ v - \sqrt{\left(\frac{H(1-\frac{\beta}{\beta_m})}{\alpha\tau}\right)}\end{pmatrix}. \tag{45}$$

To obtain the average speed for the improved model, using Eqs. (15) and (33), Δf can be expressed as

$$\Delta\boldsymbol{f} = \begin{pmatrix}\Delta f_1\\ \Delta f_2\end{pmatrix} = \boldsymbol{A}(\boldsymbol{G})\Delta\boldsymbol{G}$$
$$= \begin{pmatrix}0 & 1\\ \left(\frac{H(1-\frac{\beta}{\beta_m})}{\alpha\tau}\right) - v^2 & 2v\end{pmatrix}\begin{pmatrix}\Delta\rho\\ \Delta\rho v\end{pmatrix}. \tag{46}$$

From Eq. (46), we have

$$\Delta f_2 = \left(\left(\frac{H(1-\frac{\beta}{\beta_m})}{\alpha\tau}\right) - v^2\right)\Delta\rho + 2v\Delta\rho v, \tag{47}$$

and substituting

$$C_0^2 = \int \frac{\partial}{\partial x}\left(\left(\frac{H(1-\frac{\beta}{\beta_m})}{\alpha\tau}\right)\right) \mathrm{d}x$$

in Eq. (31) gives

$$\boldsymbol{f}(\boldsymbol{G}) = \begin{pmatrix} f_1 \\ f_2 \end{pmatrix} = \begin{pmatrix} \rho v \\ \frac{(\rho v)^2}{\rho} + \rho\left(\frac{H(1-\frac{\beta}{\beta_m})}{\alpha\tau}\right) \end{pmatrix}, \tag{48}$$

so then

$$\Delta\boldsymbol{f}(\boldsymbol{G}) = \begin{pmatrix} \Delta f_1 \\ \Delta f_2 \end{pmatrix} = \begin{pmatrix} \Delta(\rho v) \\ \Delta\left(\frac{(\rho v)^2}{\rho} + \rho\left(\frac{H(1-\frac{\beta}{\beta_m})}{\alpha\tau}\right)\right) \end{pmatrix}. \tag{49}$$

Equating Eq. (47) with Δf_2 from Eq. (49), we obtain

$$\overline{v}^2\Delta\rho - 2\overline{v}\Delta\rho v + \Delta\rho v^2 = 0, \tag{50}$$

and taking the positive root gives the average speed of the proposed model as

$$\overline{v} = \frac{2\Delta\rho v + 2\sqrt{(\Delta\rho v)^2 - (\Delta\rho)(\Delta\rho v^2)}}{2\Delta\rho}. \tag{51}$$

Substituting $\Delta\rho v = \rho_{i+1}v_{i+1} - \rho_i v_i$, $\Delta\rho v^2 = \rho_{i+1}v_{i+1}^2 - \rho_i v_i^2$, and $\Delta\rho = \rho_{i+1} - \rho_i$ in Eq. (51), we obtain the average speed at the boundary of segments i and $i+1$

$$v_{i+\frac{1}{2}} = \frac{v_{i+1}\sqrt{\rho_{i+1}} + v_i\sqrt{\rho_i}}{\sqrt{\rho_{i+1}} + \sqrt{\rho_i}}. \tag{52}$$

To obtain the average speed for the PW model, using Eqs. (15) and (33), $\Delta\boldsymbol{f}$ can be expressed as

$$\Delta\boldsymbol{f} = \begin{pmatrix} \Delta f_1 \\ \Delta f_2 \end{pmatrix} = \boldsymbol{A}(\boldsymbol{G})\Delta\boldsymbol{G} = \begin{pmatrix} 0 & 1 \\ C_0^2 - v^2 & 2v \end{pmatrix}\begin{pmatrix} \Delta\rho \\ \Delta\rho v \end{pmatrix}. \tag{53}$$

From Eq. (53), we obtain

$$\Delta f_2 = (-v^2 + C_0^2)\Delta\rho + 2v\Delta\rho v, \tag{54}$$

and using Eq. (31) gives

$$\boldsymbol{f}(\boldsymbol{G}) = \begin{pmatrix} f_1 \\ f_2 \end{pmatrix} = \begin{pmatrix} (\rho v) \\ \left(\frac{(\rho v)^2}{\rho} + C_0^2\rho\right) \end{pmatrix}, \tag{55}$$

so then

$$\Delta\boldsymbol{f}(\boldsymbol{G}) = \begin{pmatrix} \Delta f_1 \\ \Delta f_2 \end{pmatrix} = \begin{pmatrix} \Delta(\rho v) \\ \Delta\left(\frac{(\rho v)^2}{\rho} + C_0^2\rho\right) \end{pmatrix}. \tag{56}$$

Equating Eq. (54) with Δf_2 in Eq. (56) results in

$$\overline{v}^2\Delta\rho - 2\overline{v}\Delta\rho v + \Delta\rho v^2 = 0. \tag{57}$$

The average density $\rho_{i+\frac{1}{2}}$ at the boundary of segments i and $i+1$ is given by the geometric mean of the densities in these segments

$$\rho_{i+\frac{1}{2}} = \sqrt{\rho_{i+1}\rho_i}. \tag{58}$$

The eigenvalues of the Jacobian matrix $\boldsymbol{A}(\boldsymbol{G}_{i+\frac{1}{2}})$ of the proposed model are

$$\lambda_{1,2} = v_{i+\frac{1}{2}} \pm \sqrt{\left(\frac{H(1-\frac{\beta}{\beta_m})}{\alpha\tau}\right)}. \tag{59}$$

The eigenvalues of the Jacobian matrix for the PW model are

$$\lambda_{1,2} = v_{i+\frac{1}{2}} \pm C_0, \tag{60}$$

so the change in speed due to a transition is a constant. The corresponding eigenvectors are

$$\boldsymbol{e}_{1,2} = \begin{pmatrix} 1 \\ v_{i+\frac{1}{2}} \pm C_0 \end{pmatrix}. \tag{61}$$

5. Entropy fix

Entropy fix is applied to the Roe technique to smooth any discontinuities at the segment boundaries. The Jacobian matrix $\boldsymbol{A}(\boldsymbol{G}_{i+\frac{1}{2}})$ is decomposed into eigenvalues and eigenvectors to approximate the flux in the road segments in Eq. (18). Thus, the Jacobian matrix for the road segments is replaced with the entropy fix solution given by

$$\boldsymbol{e}|\boldsymbol{\Lambda}|\boldsymbol{e}^{-1},$$

where $|\boldsymbol{\Lambda}| = \left[\hat{\lambda}_1, \hat{\lambda}_2, \ldots, \hat{\lambda}_k, \ldots, \hat{\lambda}_n\right]$ is a diagonal matrix which is a function of the eigenvalues λ_k of the Jacobian matrix, and $\boldsymbol{e}$ is the corresponding eigenvector matrix. The Harten and Hayman entropy fix scheme[38] is employed here and is given by

$$\hat{\lambda}_k = \begin{cases} \hat{\delta}_k, & \text{if} \quad |\lambda_k| < \hat{\delta}_k, \\ |\lambda_k|, & \text{if} \quad |\lambda_k| \geq \hat{\delta}_k, \end{cases} \tag{62}$$

with

$$\hat{\delta}_k = \max\left(0, \quad \lambda_{i+\frac{1}{2}} - \lambda_i, \quad \lambda_{i+1} - \lambda_{i+\frac{1}{2}}\right). \tag{63}$$

This ensures that the $\hat{\lambda}_k$ are not negative and are similar at the segment boundaries. For the proposed model, we obtain

$$\begin{aligned} &\boldsymbol{e}|\boldsymbol{\Lambda}|\boldsymbol{e}^{-1} \\ &= \begin{pmatrix} 1 & 1 \\ v_{i+\frac{1}{2}} + \sqrt{\left(\frac{H(1-\frac{\beta}{\beta_m})}{\alpha\tau}\right)} & v_{i+\frac{1}{2}} - \sqrt{\left(\frac{H(1-\frac{\beta}{\beta_m})}{\alpha\tau}\right)} \end{pmatrix} \\ &\times \begin{pmatrix} \left|v_{i+\frac{1}{2}} + \sqrt{\left(\frac{H(1-\frac{\beta}{\beta_m})}{\alpha\tau}\right)}\right| & 0 \\ 0 & \left|v_{i+\frac{1}{2}} - \sqrt{\left(\frac{H(1-\frac{\beta}{\beta_m})}{\alpha\tau}\right)}\right| \end{pmatrix} \\ &\times \begin{pmatrix} v_{i+\frac{1}{2}} - \sqrt{\left(\frac{H(1-\frac{\beta}{\beta_m})}{\alpha\tau}\right)} & -1 \\ -vr_{i+\frac{1}{2}} - \sqrt{\left(\frac{H(1-\frac{\beta}{\beta_m})}{\alpha\tau}\right)} & 1 \end{pmatrix} \times \frac{-1}{2\sqrt{\left(\frac{H(1-\frac{\beta}{\beta_m})}{\alpha\tau}\right)}}, \end{aligned}$$

and for the PW model, we have

$$e|\Lambda|e^{-1} = \begin{pmatrix} 1 & 1 \\ v_{i+\frac{1}{2}}+C_0 & v_{i+\frac{1}{2}}-C_0 \end{pmatrix} \times \begin{pmatrix} \left|v_{i+\frac{1}{2}}+C_0\right| & 0 \\ 0 & \left|v_{i+\frac{1}{2}}-C_0\right| \end{pmatrix} \times \begin{pmatrix} v_{i+\frac{1}{2}}-C_0 & -1 \\ -v_{i+\frac{1}{2}}-C_0 & 1 \end{pmatrix} \frac{-1}{2C_0}.$$

The corresponding flux is obtained from Eq. (18) using $\boldsymbol{f}(\boldsymbol{G}_i)$ and $\boldsymbol{f}(\boldsymbol{G}_{i+1})$ and substituting $e|\Lambda|e^{-1}$ for $\boldsymbol{A}(\boldsymbol{G}_{i+\frac{1}{2}})$. The updated data variables ρ and ρv are then obtained at time n using Eq. (19).

6. Simulation results

The performance of the proposed and PW models is evaluated in this section using the parameters given in Table 2. Periodic boundary conditions are used to evaluate the traffic evolution on a circular road. The total simulation time for the proposed model is 75 s in both Examples 1 and 2, whereas the PW model is evaluated for 300 s in Example 1. The PW model is evaluated for a larger time to determine if the variations in the traffic flow are reduced over time as a large variation is observed at 20 s.

Table 2. Simulation parameters.

Parameter	Symbol	Value
Equilibrium velocity distribution	$v(\rho)$	Greenshields distribution
Length of road	x_M	3000 m
Maximum normalized density	$\rho_{\rm m}$	1
Maximum severity index	$\beta_{\rm m}$	1
Relaxation time	τ	0.5 s
Safe time headway	α	2 s
Example 1:		
Total simulation time for the proposed model	t_N	75 s
Total simulation time for the PW model	t_N	300 s
Number of time steps for the proposed model	N	$75/1.25 = 60$
Safe distance headway for the proposed model	H	25 m
Severity index	β	0.5
Road step for the proposed and PW models	δx	60 m
Time step for the proposed and PW models	δt	1.5 s
Number of time steps for the PW model	N	$300/1.5 = 200$
Maximum velocity for the proposed and PW models	$v_{\rm m}$	20 m/s
Velocity constant	C_0	10 m/s
Example 2:		
Maximum velocity for the proposed and PW models	$v_{\rm m}$	25 m/s
Total simulation time for the proposed model	t_N	75 s
Time step for the proposed model	δt	1.5 s
Road step for the proposed model	δx	60 m
Number of time steps for the proposed model	N	$75/1.5 = 50$
Safe distance headway for the proposed model	H	58 m
Severity index	β	0.0, 0.15, 0.95

The proposed and PW models are evaluated with $v_{\rm m} =$ 20 m/s and 25 m/s in Examples 1 and 2, respectively. The initial velocity distribution at $t = 0$ is the Greenshields equilibrium velocity distribution given by Eq. (3).[29] In Example 1, the safe distance headway is $H = 25$ m, whereas in Example 2 the safe distance headway is $H = 58$ m.[39] A smaller safe distance headway is used in Example 1 to provide a scenario with short distances between vehicles. For both examples, $\alpha = 2$ s.

Both models are evaluated using a relaxation time of $\tau =$ 0.5 s, which is suitable for transitions over small distances.[40] Further, a small value of δx is used to ensure accurate numerical results. Therefore, the road of length $x_M = 3000$ m is divided into $M = 50$ equal segments with $\delta x = 60$ m for both models. To satisfy the CFL condition,[41] $\delta t = 1.25$ s is employed in Example 1 and $\delta t = 1.5$ s in Example 2 for the proposed model. Then $t_N = 75$ s is divided into $N = 60$ and $N = 50$ intervals in Examples 1 and 2, respectively. For the PW model, $t_N = 300$ s and is divided into $N = 200$ intervals. The initial density ρ_0 at time $t = 0$ s for Example 1 has the following distribution:

$$\rho_0 = \begin{cases} 0.01, & \text{for} \quad x \le 500; \\ 0.3, & \text{for} \quad 500 < x \le 1300; \\ 0.1, & \text{for} \quad 1300 < x \le 1750; \\ 0.01, & \text{for} \quad x > 1750, \end{cases} \tag{64}$$

which spans the first 3000 m of the road. The maximum density is $\rho_m = 1$, which means that the road is 100% occupied. The initial density ρ_0 at time $t = 0$ s for Example 2 has the following distribution:

$$\rho_0 = \begin{cases} 0.05, & \text{for} \quad x \leq 500; \\ 0.3, & \text{for} \quad 500 < x \leq 1300; \\ 0.15, & \text{for} \quad 1300 < x \leq 1750; \\ 0.05, & \text{for} \quad x > 1750, \end{cases} \tag{65}$$

which spans the first 3000 m of the road. The velocity constants used in the literature for the PW model vary between 2.4 m/s and 57 m/s to evaluate the performance with different traffic densities.[28,42,43] Thus the value of C_0 considered here is 10 m/s.

6.1. Example 1

In this example, the traffic behavior in the proposed model is evaluated for $\beta = 0.5$. Figure 1 presents the traffic density with the proposed model over a time span of 75 s for the 50 road steps. At the 60th time step (after 75 s), the traffic density is highest between the 30th and 40th road steps with a maximum of 0.25, so the headway between vehicles is small. The density gradually reduces from 0.25 at the 37th road step to 0.1 at the 50th road step, so the headway between vehicles increases. The minimum traffic density of 0.01 occurs from the 15th to 30th road steps. The maximum change of 0.19 occurs between the 30th and 40th road steps. This is a smaller variation in density than with the PW model as shown in Fig. 2.

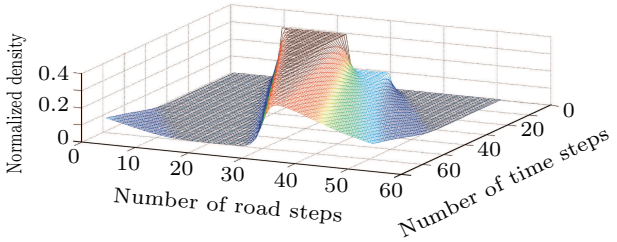


Fig. 1. (color online) The proposed model density behavior on a circular road with $\beta = 0.5$, relaxation time $\tau = 0.5$ s, safe time headway $\alpha = 2$ s, and safe distance headway $H = 25$ m.

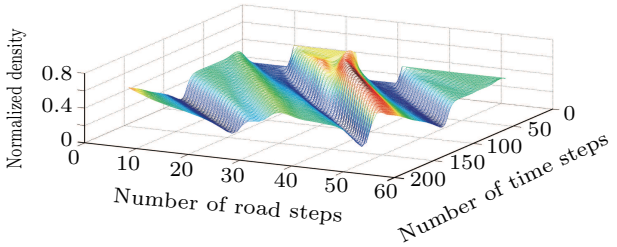


Fig. 2. (color online) The PW model density behavior with $C_0 = 10$ m/s on a circular road.

The traffic density behavior on the circular road over a time span of 300 s with the PW model is given in Fig. 2. The density at the 150th time step reaches 0.6 at the 35th road step. For a density of 0.6, the headway is small and the changes in velocity are high as observed in Fig. 4. The change in traffic density between the 0th and 30th road steps is large. At 300 s (150th time step), the density at the 0th road step is 0.6 and reduces to 0.2 at the 30th road step and then changes to 0.4 at the 32nd road step. The density at the 150th time step changes from 0.2 at the 48th road step to 0.8 at the 50th road step, and exhibits oscillatory behavior, which is unrealistic.

The velocity behavior on the circular road over a time span of 75 s with the proposed model is given in Fig. 3. At the 60th time step (after 75 s), the velocity is 15 m/s at the 37th road step, which is the minimum velocity. At the 60th time step, the velocity increases gradually from 15 m/s at the 37th road step to 18 m/s at the 50th road step. The maximum velocity of 20 m/s occurs at the 60th time step from the 15th to 30th road steps. The maximum variation of 5 m/s occurs at the 60th time step between the 30th and 40th road steps, which is smaller than that with the PW model as shown in Fig. 4.

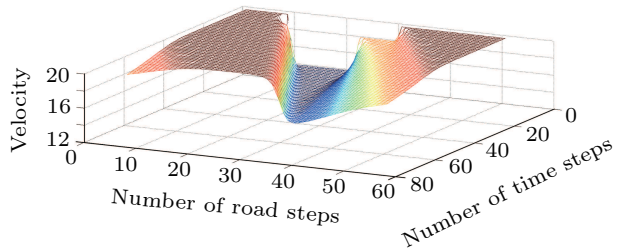


Fig. 3. (color online) The proposed model velocity behavior on a circular road with $\beta = 0.5$, relaxation time $\tau = 0.5$ s, safe time headway $\alpha = 2$ s, and safe distance headway $H = 25$ m.

The velocity behavior on the circular road over a time span of 300 s with the PW model is given in Fig. 4. This shows that the velocity reaches 30 m/s even though 20 m/s is the maximum possible velocity. Further, there are drastic changes in velocity between the 25th and 30th road steps at the 150th time step. The velocity varies from 15 m/s at the 25th road step to 25 m/s at the 30th road step. This change of 10 m/s in velocity within 5 road steps is not realistic. With the proposed model, the variations in velocity are much smaller than those with the PW model.

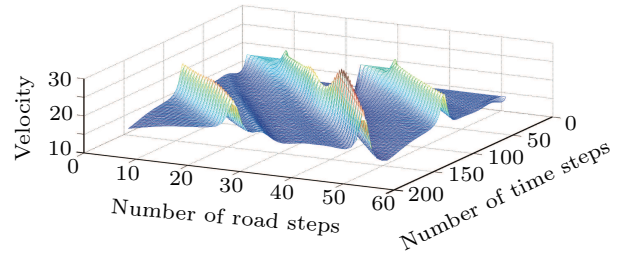


Fig. 4. (color online) The PW model velocity behavior with $C_0 = 10$ m/s on a circular road.

The traffic flow behavior with the proposed model over a time span of 75 s for the 50 road steps is presented in Fig. 5.

At the 60th time step (after 75 s), the traffic flow is high between the 30th and 40th road steps and attains a maximum of 3.75 veh/s. At the 60th time step, the traffic flow gradually reduces from 3.75 veh/s at the 37th road step to 2 veh/s at the 50th road step. The minimum traffic flow of 0.2 veh/s occurs at the 60th time step from the 15th to 30th road steps. The maximum variation of 1.75 veh/s occurs at the 60th time step between the 30th and 40th road steps, which is smaller than with the PW model as shown in Fig. 6.

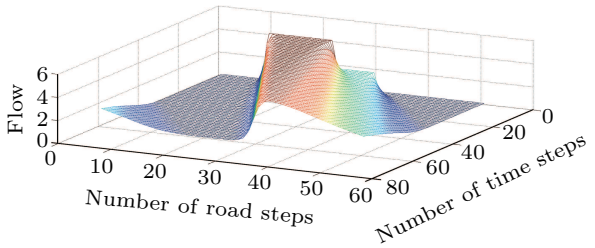


Fig. 5. (color online) The proposed model flow behavior on a circular road with $\beta = 0.5$, relaxation time $\tau = 0.5$ s, safe time headway $\alpha = 2$ s, and safe distance headway $H = 25$ m.

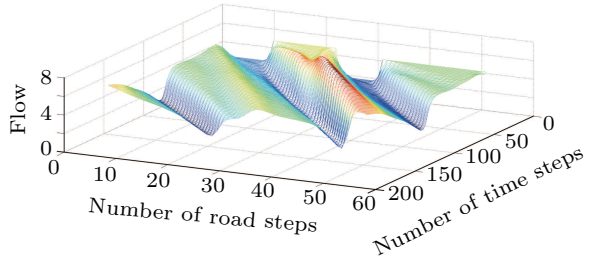


Fig. 6. (color online) The PW model flow behavior with $C_0 = 10$ m/s on a circular road.

The traffic flow behavior on the circular road over a time span of 300 s with the PW model is given in Fig. 6. At the 50th time step, the maximum flow of 8 veh/s occurs at the 30th road step. The flow varies from 2 veh/s at the 20th road step to 8 veh/s at the 30th road step at this time. The traffic flow at the 150th time step with the PW model reaches 6 veh/s at the 35th road step. The change in traffic flow between the 0th and 30th road steps is large. At 300 s (150th time step), the flow at the 0th road step is 6 veh/s and reduces to 2 veh/s at the 30th road step, and then changes to 4 veh/s at the 32nd road step. The flow changes from 2 veh/s at the 48th road step to 8 veh/s at the 50th road step, and exhibits oscillatory behavior, which is unrealistic.

The results in Figs. 2, 4, and 6 show that the PW model does not accurately characterize the traffic flow. The variations in traffic flow are larger than those with the proposed model. Further, the proposed model results in velocities between 0 m/s and 20 m/s, whereas the velocity with the PW model exceeds the maximum. The variations in traffic flow and velocity are small with the proposed model, which is expected in adverse weather.

6.2. Example 2

Figure 7 presents the traffic density behavior at 75 s with both the PW and proposed models on a circular road of length 3000 m. The proposed model traffic flow behavior is given for $\beta = 0, 0.15$, and 0.95, corresponding to three different weather conditions. $\beta = 0$ represents normal weather, $\beta = 0.15$ characterizes low adverse weather, and $\beta = 0.95$ indicates severe adverse weather.

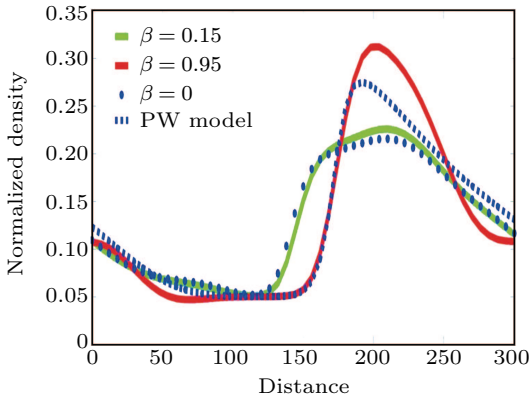


Fig. 7. (color online) The proposed model density behavior with $\beta = 0.0$, 0.15, and 0.95, safe time headway $\alpha = 2$ s, and safe distance headway $H = 58$ m at 75 s, on a circular road of length 3000 m. The PW model density behavior with $C_0 = 10$ m/s is also given.

The traffic density with $\beta = 0.95$ increases from 0.05 at 1500 m to 0.32 at 2000 m and then reduces to 0.12 at 2700 m at 75 s. The traffic density varies from 0.12 at 2900 m to 0.05 at 500 m. The maximum density is 0.32 at 2000 m. This indicates that the headway is small at 2000 m with $\beta = 0.95$. The density is approximately 0.05 between 500 m and 1500 m, which is the minimum density with $\beta = 0.95$. With $\beta = 0.15$, the density gradually reduces from 0.12 at 0 m to 0.05 at 1300 m and then gradually increases to 0.23 at 2400 m, which then reduces to 0.12 at 3000 m. The maximum density variation of 0.27 with $\beta = 0.95$ occurs between 1500 m and 2000 m, whereas with $\beta = 0.15$, the maximum density variation of 0.11 occurs between 1300 m and 2400 m. This indicates that a smaller variation in density occurs over a larger distance in low adverse weather compared to that in severe adverse weather. In normal weather ($\beta = 0$), the traffic density is smoother than that with $\beta = 0.15$. The maximum density is 0.21 with $\beta = 0$ which is less than the 0.23 with $\beta = 0.15$. The majority of vehicles with the PW model are between 1500 m and 700 m on the circular road. The density varies from 0.05 at 1500 to 0.27 at 1800 m and then reduces to 0.05 at 700 m. This large change in density (0.22) occurs over a small distance of 300 m and then reduces gradually to 0.05 over a distance of 1900 m. These results show that the proposed model can characterize traffic behavior in different weather conditions whereas the PW model exhibits the same behavior in all weather conditions.

Figure 8 presents the traffic density behavior with the proposed model on a circular road over a time span of 75 s with $\beta = 0.15$. In low adverse weather, the density of 0.29 at $t = 0$ s gradually reduces to 0.11 at 75 s. The maximum density at 75 s is 0.23 at 2400 m. A variation in density of 0.11 occurs between 1300 m and 2400 m. Figure 9 presents the corresponding traffic density behavior with $\beta = 0.95$. The maximum change in density of 0.27 occurs between 1500 m and 2000 m, and the maximum density is 0.32 at 2000 m. This shows that in severe adverse weather, the traffic is spread over a smaller distance with a larger variation in density than in low adverse weather.

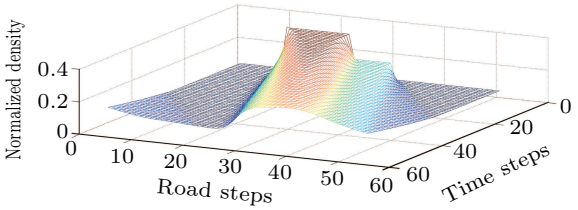


Fig. 8. (color online) The proposed model density behavior with $\beta = 0.15$, safe time headway $\alpha = 2$ s, and safe distance headway $H = 58$ m on a circular road of length 3000 m.

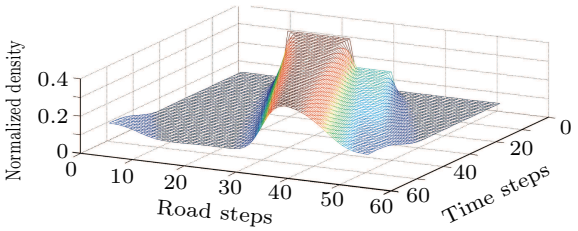


Fig. 9. (color online) The proposed model density behavior with $\beta = 0.95$, safe time headway $\alpha = 2$ s, and safe distance headway $H = 58$ m on a circular road of length 3000 m.

The traffic velocity at 75 s is shown in Fig. 10 for $\beta = 0.15$ and 0.95. For $\beta = 0.95$, the fastest traffic is between 500 m and 1000 m with a maximum velocity of 24 m/s, and the slowest traffic is between 1800 m and 2300 m with a maximum velocity of 18 m/s. With $\beta = 0.15$, the velocity reaches 25 m/s between 500 m and 700 m. The traffic attains the maximum velocity as the surface friction is larger than that with $\beta = 0.95$. The velocity with $\beta = 0.15$ ranges from 25 m/s at 500 m to 16 m/s at 1600 m, while with $\beta = 0.95$ it ranges from 24 m/s at 1000 m to 18 m/s at 2000 m. The variation in velocity is 6 m/s with $\beta = 0.95$, while with $\beta = 0.15$ it is 9 m/s. Smaller changes in velocity are expected in more adverse weather.

The traffic flow with the proposed model on a circular road of 3000 m for $\beta = 0.15$ and 0.95 at 75 s is presented in Fig. 11. The traffic flow with $\beta = 0.95$ increases from 1.2 veh/s at 1500 m to 5.8 veh/s at 2000 m and then reduces to 2.2 veh/s at 2700 m. The traffic flow varies from 2.2 veh/s at 2700 m to 1.1 veh/s at 500 m. The maximum flow is 5.8 veh/s at 2000 m. The traffic flow is approximately 1.1 veh/s between 500 m and 1500 m, which is the minimum flow with $\beta = 0.95$. With $\beta = 0.15$, the traffic flow gradually reduces from 2.15 veh/s at 0 m to 1.1 veh/s at 1300 m and then gradually increases to 4.0 veh/s at 2400 m, which then reduces to 2.2 veh/s at 3000 m. With $\beta = 0.95$, the variation in flow is 4.7 veh/s between 1500 m and 2000 m, whereas with $\beta = 0.15$, the variation in flow is 2.9 veh/s between 1300 m and 2400 m. This indicates that smaller variations in flow occur in low adverse weather compared to in severe adverse weather.

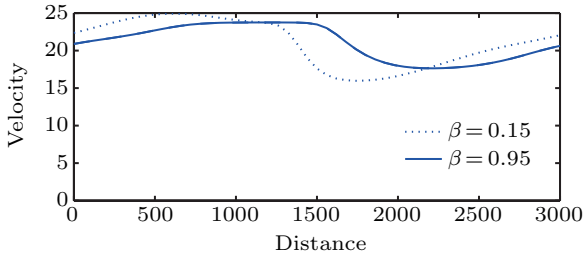


Fig. 10. (color online) The proposed model velocity behavior with $\beta = 0.15$ and 0.95, safe time headway $\alpha = 2$ s, and safe distance headway $H = 58$ m at 75 s on a circular road of length 3000 m.

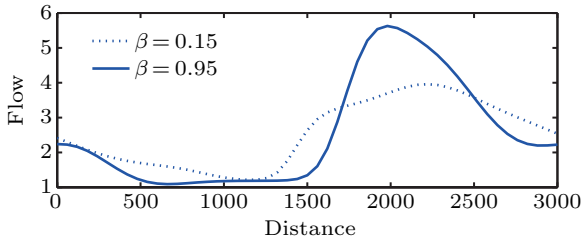


Fig. 11. (color online) The proposed model flow behavior with $\beta = 0.15$ and 0.95, safe time headway $\alpha = 2$ s, and safe distance headway $H = 58$ m at 75 s on a circular road of length 3000 m.

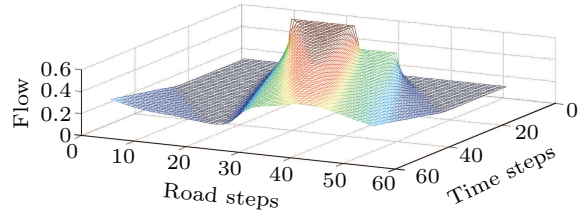


Fig. 12. (color online) The proposed model flow behavior with $\beta = 0.15$, safe time headway $\alpha = 2$ s, and safe distance headway $H = 58$ m on a circular road of length 3000 m.

The traffic flow behavior over a circular road of 3000 m with $\beta = 0.15$ and 0.95 over a time span of 75 s is presented in Figs. 12 and 13, respectively. Figure 12 shows that with $\beta = 0.15$, the variation in flow after 75 s is 2.9 veh/s with a maximum flow of 4 veh/s at 2400 m. Figure 13 shows that with $\beta = 0.95$, the variation in flow is 4.7 veh/s with a maximum flow of 5.8 veh/s at 2000 m. A large variation in flow over time is expected in more adverse weather. Thus as the severity increases, the majority of the vehicles are located over a smaller distance and there is a smaller variation in velocity.

This example shows that the proposed model can characterize the traffic under different weather conditions. The PW model has the same response for all weather conditions and so cannot characterize traffic during adverse weather.

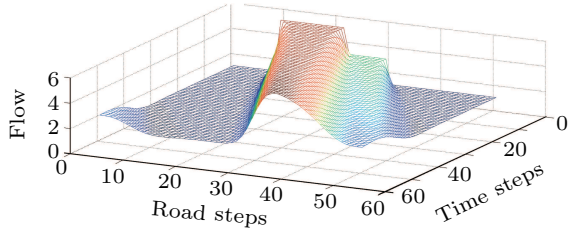


Fig. 13. (color online) The proposed model flow behavior with $\beta = 0.95$, safe time headway $\alpha = 2$ s, and safe distance headway $H = 58$ m on a circular road of length 3000 m.

7. Conclusion

Adverse weather has a significant impact on traffic behavior and driving safety. Tire friction on a road is reduced with snow, ice, and compacted snow, which leads to a higher accident rate. In this paper, a model was developed to characterize traffic flow based on the surface conditions of the road. In adverse weather, traffic with the proposed model has less variations in velocity and density than with the PW model, which is more realistic. Further, traffic with the PW model has oscillatory behavior and the velocity shows drastic changes, which is not expected in adverse weather conditions. In adverse weather, drivers are cautious so small changes in density and velocity are expected. With the proposed model, traffic becomes smoother over time than that with PW model, which is more realistic. In addition, the variations in velocity are not as large as those with the PW model and stay within the velocity limits. The small variations in traffic density and velocity with the proposed model during adverse weather are a better characterization of traffic flow. The PW model cannot characterize traffic flow in different weather conditions due to the use of constant density changes for all conditions. Conversely, the proposed model employs a severity index based on road surface conditions to characterize the traffic flow according to the weather.

References

[1] Khan Z H 2016 *Traffic Flow Modelling for Intelligent Transportation Systems* (Ph.D. Dissertation) (Canada: University of Victoria)
[2] Khan Z H and Gulliver T A 2018 *European Transport Research Review* **10** 30
[3] Elevant K 2013 *Intelligent Transportation Systems* **7** 415
[4] Hassan H M and Abdel-Aty M A 2011 *Transportation Research F* **14** 614
[5] Pisano P A and Goodwin L C 2004 *J. Transportation Research Board* **1867** 127
[6] Theofilatos A and Yannis G 2014 *Accident Analysis and Prevention* **72** 244
[7] Lee W K, Lee H A, Hwang S S, Kim H, Lim Y H, Hong Y C, Eh H and Park H 2015 *J. Epidemiology* **25** 544
[8] Goodwin L C 2002 *Proceedings of Road Weather Management* VA, USA
[9] Qiu L and Nixon W A 2008 *Transportation Research Record* **2055** 139
[10] Weng J, Liu L and Rong J 2012 *Discrete Dynamics in Nature and Society* **2013** 1
[11] McBride J C 1997 *Economic Impact of Highway Snow and Ice Control. Federal Highway Administration* Washington, D.C.
[12] Ibrahim A T and Hall F L 1994 *Transportation Research Record* **1457** 184
[13] Maki P J 1999 *Proceedings of 69th Annual Meeting of the Institute of Transportation Engineers* August 1–4, 1999, Las Vegas, Nev., USA
[14] Lighthill M J and Whitham J B 1955 *Proceedings of Royal Society A* **229** 317
[15] Richards P I 1956 *Operations Research* **4** 42
[16] Zhang H 1998 *Transportation Research Board* **32** 485
[17] Payne H J 1971 *Simulation Council Proceedings* **1** 51
[18] Jin W L and Zhang H M 2003 *Transportation Research B* **37** 207
[19] Chen J, Peng Z and Fang Y 2015 *Mod. Phys. C* **29** 1550017
[20] Gupta A K, Sharma S and Redhu P 2014 *Commun. Theor. Phys.* **62** 393
[21] Hong H, Wei L, Yu X and Li D 2009 *Chin. Phys. B* **18** 2703
[22] Kaur R and Sharma S 2018 *Physica A* **499** 110
[23] Meng X P and Yan L Y 2017 *Asian J. Control* **19** 1844
[24] Zhu W X and Yu R L 2014 *Physica* **393** 101
[25] http://www.zjemw.com/safeDriving/ShowSafeDriving.asp?
[26] Xing L, Tao S, Hua K and Shi D 2008 *Chin. Phys. B* **17** 3014
[27] Chen J, Shi Z, Hu Y, Yu L and Fang Y 2013 *Int. J. Modern Phys. C* **24** 1350061
[28] Morgan J V 2002 *Numerical Methods for Macroscopic Traffic Models* (Ph.D. Dissertation) (UK: University of Reading, Berkshire)
[29] Greenshield B D 1935 *Proceedings of Highway Research Board* **14** 448
[30] Muralidharan A 2012 *Tools for Modeling and Control of Freeway Networks* (Ph.D. Dissertation) (Berkeley: University of California Berkeley)
[31] Strong C k, Ye Z and Shi X 2009 *Transportation Review* **30** 677
[32] Kurganov A, Noelle S and Petrova G 2001 *Siam J. Sci. Comput.* **23** 707
[33] Chen J Z, Shi Z K and Hu Y M 2009 *J. Zhejiang University-Science A* **10** 1835
[34] Chen J Z, Shi Z K and Hu Y M 2012 *J. Zhejiang University-Science C* **13** 29
[35] Guang J and Chi S 1996 *J. Comput. Phys.* **126** 202
[36] Kachroo P, Al-Nasur S J, Wadoo S A and Shende A 2008 *Pedestrian Dynamics: Feedback Control of Crowd Evacaution* (Berlin Heidelberg: Springer-Verlag Berlin Heidelberg) p. 66
[37] Roe P L 1981 *J. Comput. Phys.* **43** 357
[38] Harten A and Hayman J M 1983 *J. Comput. Phys.* **50** 253
[39] Risto M and Martens M H 2013 *Transportation Research F* **15** 45
[40] Basak K, Hetu S N, Li Z, Azevedo C L, Loganathan H, Toledo T, Xu R, Xu Y, Peh L S, and Ben-Akiva M 2013 *Proceedings of 16th International IEEE Conference on intelligent Transportation Systems* October 6–9, 2013 The Hague, The Netherlands, p. 302
[41] LeVeque R J 1992 *Numerical Methods for Conservation Laws* (2nd Edn.) (Basel: ETH Zürich, Birkhäuser Verlag) pp. 149–156
[42] Wenlog J 2000 *Traffic Flow Models and Their Numerical Solutions* (Masters thesis) (Davis: University of California Davis)
[43] Wenlog J and Zhang H M 2001 *Technical Report* (Davis: University of California Davis)